



DIE ERDE

Journal of the
Geographical Society
of Berlin

BioCAS: Biometeorological Climate impact Assessment System for building-scale impact assessment of heat-stress related mortality

Kyu Rang Kim¹, Chaeyeon Yi², Ji-Sun Lee¹, Fred Meier³, Britta Jänicke³, Ute Fehrenbach³, Dieter Scherer³

¹ National Institute of Meteorological Research, 33 Seohobuk-ro, Seogwipo-si, Jeju-do 697-845, Republic of Korea, krk9@kma.go.kr, ljsun6@korea.kr

² WISE (Weather Information Service Engine) Project, 12 Fl. 434 Worldcupbuk-ro, Mapo-gu, Seoul 121-835, Republic of Korea, prpr.chaeyeon@gmail.com

³ Technische Universität Berlin, Rothenburgstr. 12, 12165 Berlin, Germany, Fred.Meier@tu-berlin.de, Britta.Jaenicke@tu-berlin.de, Ute.Fehrenbach@tu-berlin.de, Dieter.Scherer@tu-berlin.de

Manuscript submitted: 20 July 2013 / Accepted for publication: 17 June 2014 / Published online: 2 September 2014

Abstract

An urban climate analysis system for Seoul was combined with biometeorological models for the spatially distributed assessment of heat stress risks. The Biometeorological Climate impact Assessment System (BioCAS) is based on the Climate Analysis Seoul (CAS) workbench which provides urban planners with gridded data relevant for local climate assessment at 25 m and 5 m spatial resolutions. The influence of building morphology and vegetation on mean radiant temperature T_{mrt} was simulated by the SOLWEIG model. Gridded hourly perceived temperature PT was computed using the Klima-Michel Model for a hot day in 2012. Daily maximum perceived temperature PT_{max} was then derived from these data and applied to an empirical-statistical model that explains the relationship between PT_{max} and excess mortality rate r_{EM} in Seoul. The resultant r_{EM} map quantifies the detrimental impact of hot weather at the building scale. Mean (maximum) values of r_{EM} in old and new town areas in an urban re-development site in Seoul were estimated at 2.3 % (50.7 %) and 0 % (8.6 %), respectively, indicating that urban re-development in the new town area has generally resulted in a strong reduction of heat-stress related mortality. The study illustrates that BioCAS can generally be applied for the quantification of the impacts of hot weather on human health for different urban development scenarios. Further improvements are required, particularly to consider indoor climate conditions causing heat stress, as well as socio-economic status and population structure of local residents.

Zusammenfassung

Ein System zur Stadtklimaanalyse von Seoul wurde mit biometeorologischen Modellen kombiniert, um eine räumlich verteilte Abschätzung von Hitzestressrisiken durchzuführen. Das Biometeorologische Klimafolgen-Assessment-System (BioCAS) basiert auf einer Arbeitsumgebung für die Klimaanalyse Seoul (CAS), welche der Stadtplanung Rasterdaten mit räumlichen Auflösungen von 25 m und 5 m bereitstellt, die für eine Abschätzung der lokalen Klimabedingungen relevant sind. Der Einfluss von Gebäudemorphologie und Vegetation auf die mittlere Strahlungstemperatur T_{mrt} wurde mittels des SOLWEIG-Modells simuliert. Stündliche Rasterdaten zur Gefühlten Temperatur PT wurden mittels des Klima-Michel-Modells für einen heißen Tag im Jahr 2012 berechnet. Daraus wurde das räumliche Muster des Maximums der Gefühlten Temperatur PT_{max} ermittelt und für ein empirisch-statistisches Modell verwendet, das den Zusammenhang zwischen PT_{max} und der Überschussmortalitätsrate r_{EM} in Seoul erklärt. Die daraus resultierende r_{EM} -Karte quantifiziert die verheerenden Auswirkungen hoher Lufttemperaturen auf der Gebäudeskala. Für Alt- und Neustadtgebiete wurden mittlere (maximale) r_{EM} -Werte

Kim, Kyu Rang, Chaeyeon Yi, Ji-Sun Lee, Fred Meier, Britta Jänicke, Ute Fehrenbach and Dieter Scherer 2014: BioCAS: Biometeorological Climate impact Assessment System for building-scale impact assessment of heat-stress related mortality. – DIE ERDE 145 (1-2): 62-79



DOI: 10.12854/erde-145-6

von 2.3 % (50.7 %) bzw. 0 % (8.6 %) ermittelt, was ein Indikator dafür ist, dass die Sanierungsmaßnahmen im Neustadtgebiet zu einer allgemeinen Reduktion der mit Hitzestress verbundenen Mortalität geführt hat. Diese Studie illustriert die generelle Anwendbarkeit des BioCAS zur Quantifizierung der Auswirkungen hoher Lufttemperaturen auf die menschliche Gesundheit für unterschiedliche Stadtentwicklungsszenarien. Weitere Verbesserungen sind erforderlich, insbesondere, um Innenraumklimabedingungen, die Hitzestress verursachen, sowie den sozioökonomischen Status und die Bevölkerungsstruktur der lokalen Anwohner zu berücksichtigen.

Keywords Urban planning, urban development, urban heat island, biometeorology, meteorological environmental impact assessment

1. Introduction

Urban areas with dense population show a higher air temperature than surrounding suburban or rural areas, which is known as urban heat island (UHI) (Oke 1973). UHI intensity, observed in 31 cities in US California, became more evident since the 1940s. The UHI situation aggravated with higher building density and increasing energy consumption along with less vegetation in urban areas in addition to climate change (Akbari et al. 1992). Korea also experienced a significant increase of the daily maximum temperature in major urban areas since the 1960s (NIMR 2009). Megacities like Seoul are thermally overloaded by building structure, reduced latent heat flux and increased heat storage during daytime, and subsequent increased sensible heat flux into the urban atmosphere during nighttime, along with increased anthropogenic heat from air conditioning systems and vehicles (Tran et al. 2006, Narumi et al. 2009).

The frequency of high temperature events in urban areas increased with the rise of global mean air temperature. This increase is correlated with elevated mortality (Kalkstein and Greene 1997). Air temperature increase can cause direct health problems such as exhaustion or heat shock with overloaded cardiovascular system, or indirect problems with respiratory organs, for instance through elevated level of photochemical smog (U.S. EPA, 2006, Gray and Finster 2000). A brief review of studies on the relations between urban climate and heat stress is given by Scherer and Endlicher (2013). Recently, increasing morbidity (Scherber et al. 2013) and mortality (Scherer et al. 2013) risks related to heat stress have been quantified for Berlin, Germany, revealing that this problem is not restricted to cities under tropical or subtropical climates.

Health issues during heat waves are also reported for Korea which is located in the temperate region of

Northeast Asia with hot and humid summers. Sudden mortality increases were observed during prolonged episodes of high air temperature in Korea – during a heat wave in 1994, the total death toll exceeded 3000 in South Korea (Kysely and Kim 2009). Several studies have addressed the relationship between elevated air temperatures and mortality in Seoul, the capital of Korea, as well as in further Korean cities. Threshold temperature of excess mortality during heat waves was in the range of 27-30 °C in Korea as determined by observed daily mortality and air temperature but based on different methods and mortality data as compared to this study. For example, the threshold temperature was determined as 29.4 °C by Kim et al. (2009b) and 28.1 °C by Kim et al. (2006). The population of Seoul and its surrounding metropolitan area exceeds 25 million people, which is about half of the national population of Korea. This high percentage reveals the high importance of urban climate impacts for public health in Korea.

In former studies, heat-stress conditions in major cities in Korea were analysed using data on perceived temperature PT , which is based on a heat budget model between the internal and external human body (Kim et al. 2009a, Staiger et al. 2012) as indicator of heat-stress conditions. Besides air temperature and relative humidity, wind speed and mean radiant temperature T_{mrt} control PT . In Korean studies, daily maximum perceived temperature PT_{max} was frequently chosen as predictor for estimating excess mortality related to heat stress (Kim et al. 2011b).

The Korea Meteorological Administration (KMA) releases heat wave warnings so that the National Emergency Management Agency (NEMA) and local governments can engage various preventive actions to reduce detrimental impacts related to high air temperature. The Heat Health Warning System (HHWS) is operational during summer for 14 larger cities in

Korea (Lee et al. 2010), so health impacts of high air temperature are considered in the heat warnings. Initially, despite its complex urban structure, the HHWS for Seoul provided warning information only for the entire city. As an improvement, the original HHWS was modified to provide regional heat warnings in Seoul by dividing the city into five regions, based on a cluster analysis of daily maximum air temperature from 25 districts. Detailed heat warnings for the five regions were provided by models for estimating excess mortality, which had been developed from daily data on death counts during heat waves, also considering layout and structure of buildings, topography, as well as population density in Seoul (Kim et al. 2011a).

From time to time, old city areas need an overhaul of the buildings for their safety, so that there is an option of re-developing some parts of old districts to a greener and more comfortable city for the everyday life of the citizens. In urban re-development or re-design planning, the economic benefit of a new development plan can readily be assessed by various ways such as the increased number of residents or the size of commercial areas, along with the estimated costs for re-development. The Seoul Metropolitan Government established an ordinance on environmental impact assessment for such re-development plans requesting from business operators to maintain the quality of the original environment (SMG 2009). Thus, the costs for re-

development could eventually exceed the economic benefits due to restrictions identified by the environmental impact assessment. Unfortunately, heat stress is not yet explicitly considered as a hazard that should be prevented by urban re-development in Korea. This is partly due to the lack of studies providing detailed assessment models for elevated air temperatures around buildings induced by changes in urban structures. Therefore, reducing heat stress for the benefit of urban people through detailed impact assessment of urban development on human health is required (Ebi et al. 2004, Harlan et al. 2006, Shahmohamadi et al. 2011).

The Climate Analysis Seoul (CAS) workbench, briefly called CAS hereafter, was developed to determine the influence of buildings and vegetation areas on near-surface air temperature and wind conditions within the Seoul metropolitan area (Yi et al. 2012). CAS defines three different nested domains as shown in Figure 1 for which gridded geographic data on topography and land cover are used as input for a suite of numerical models providing gridded data relevant for urban climate impact assessment. The Model Region (MR) covers the central part of the Korean peninsula, the Study Region (SR) covers the entire administrative area of Seoul, and the Detail Region (DR) includes an urban development area called Eunpyeong in the northwest of Seoul. The domains show strong topographic variations and include large ar-

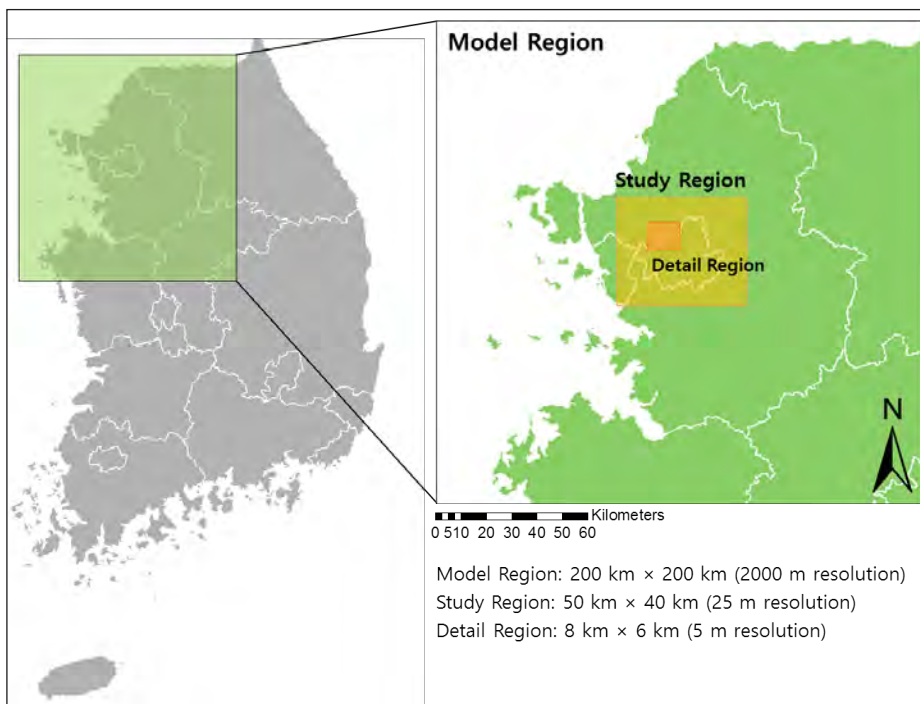


Fig.1 Nested domains of the Climate Analysis Seoul (CAS): Model Region (MR), Study Region (SR), and Detail Region (DR) Eunpyeong. Source: National Geographic Information Institute, Korea

areas covered by forests, as well as other types of vegetation in and around built-up areas.

The DR experienced urban re-development from 2006 to 2011 that transformed some parts of old town areas into new ones. Comparing the new and old towns (Fig. 2), the old one has smaller buildings covering major part of the ground area, and the space between them is mainly unvegetated. The new town has buildings more than five times taller with many small parks and green spaces between them. Tall buildings can cast shadows behind them. One of the major objectives of CAS is to assess urban climate modifications caused by urbanisation and urban re-development. However, CAS did not include a model component for estimating r_{EM} for hot days, so far.

In this study, we developed a spatially distributed system for biometeorological impact assessment (BioCAS) for Seoul to estimate excess mortality rates r_{EM} related to heat stress during hot days at the building-scale. BioCAS integrates high resolution CAS data sets and additional models for estimating spatial variations in r_{EM} between town areas of different urban characteristics.

BioCAS was tested in this study by diagnosing spatial variations in r_{EM} on August 5, 2012, the day Seoul experienced the most severe hot weather during that year. The study was carried out for the CAS DR, since there, both older city structures and re-developed ones are present. It should be noted that this study only demonstrates the feasibility of the BioCAS approach, since spatially distributed data on r_{EM} directly derived from spatially distributed death counts are not available at this high level of spatial detail.

2. Data and methods

2.1 Data

Three different types of data were used to develop the BioCAS system: records from meteorological observations, geographic data on buildings and vegetation, and daily death counts for Seoul.

In the SR, weather data from 51 automated weather stations and the Seoul Weather Station (SWS, Korea climate station #47108) of the KMA were utilised (Fig. 3). Air temperature and relative humidity at 1.5 m above ground were observed in the DR at nine sites every 15 minutes since March 2007. Ten additional sensors were installed inside the new town area in September 2010, when the construction was almost finished.

Airborne LiDAR data (ALS50, 2009, density: 2.5 points per m^2) from National Geographic Information Institute and high resolution optical satellite images (KOMPSAT-2, 2009; resolution: 4 m) from Korea Aerospace Research Institute were assimilated in CAS to produce digital terrain and surface models, as well as land cover maps for the SR and the DR at spatial resolutions of 25 m and 5 m (Yi et al. 2011 and 2012). The Shuttle Radar Topography Mission digital topographic data (SRTM, 2000; resolution: 90 m) and Moderate Resolution Imaging Spectrometer land cover data (MODIS, 2004; resolution: 1 km) from NASA were utilised for the MR at a spatial resolution of 1 km (Yi et al. 2011).

Data on daily death counts in Seoul were obtained from Statistics Korea (KOSTAT, formerly known as the



Fig. 2 Street views and maps from the old (left) and new (right) town areas in the Detail Region (DR) Eunpyeong, showing the differences of building height and spacing, vegetation area, and street density between them. Source: <http://map.Daum.net>

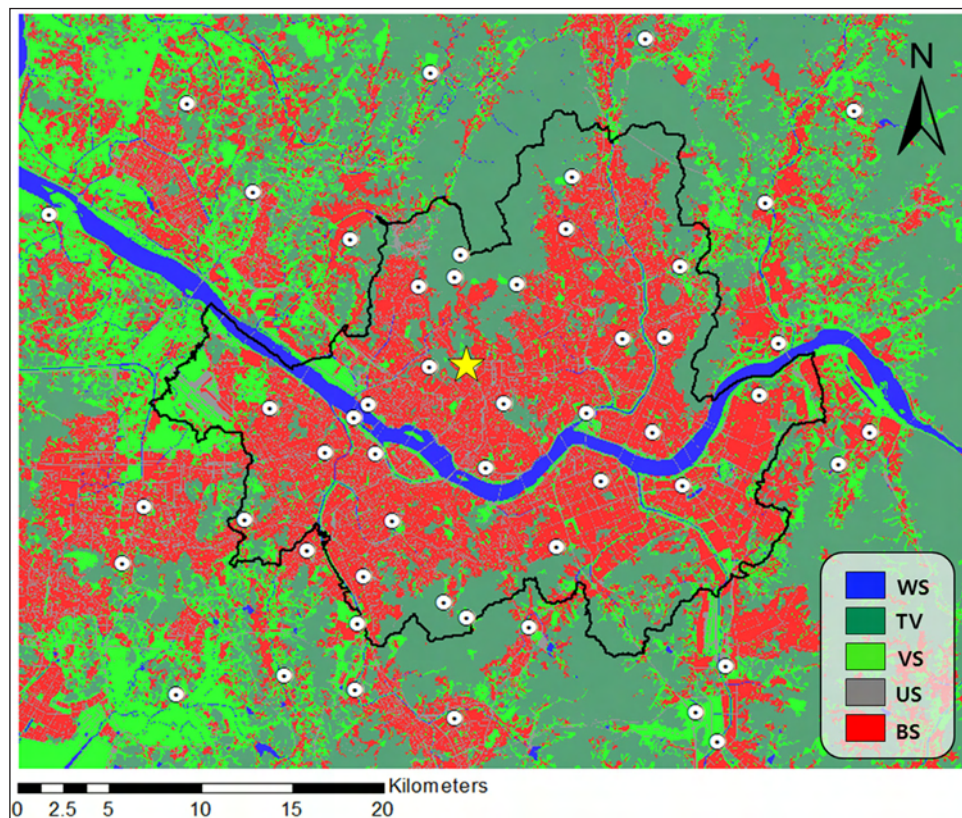


Fig. 3 Study Region (SR) of the Climate Analysis Seoul (CAS) with 51 automatic weather stations (marked by circles) and the Seoul Weather Station (SWS; marked by star), operated by the Korean Meteorological Administration (KMA) in and around Seoul. Primary land cover classes are indicated by colors (WS: water surfaces, TV: tall vegetation, VS: vegetated surfaces, US: unvegetated surfaces, BS: built-up surfaces)

National Statistics Office). Death counts are reported for different causes of death according to the International Classification of Diseases (ICD). In this study, we considered only those deaths that were caused by heat related diseases, i.e. those diseases whose symptoms can be worsened by high air temperature or are associated with indirect heat effects (see *Tab. 1*).

2.2 Methods

The model parts of BioCAS are integrated to enable the workflow shown in *Figure 4*. The individual computational steps are described in the following paragraphs.

2.2.1 Climate Analysis Seoul (CAS)

CAS consists of a database management system, both for spatially distributed GIS data and for time series from AWS observations, which are used by a suite of numerical models and diagnostic tools for simulating, analysing and visualising meso- and local-scale climate controls and weather phenomena, and their influence on urban climate. CAS provides a programmable software environment including a graphical user interface that organises data management, processing and visualisation in a consistent workflow. CAS and its model components were utilised in BioCAS for two different purposes (see *Fig. 4*).

Tab. 1 Heat related diseases and their International Classification of Diseases (ICD) codes

Code	Causes of death
E00~99	Endocrine, nutritional and metabolic disease
F00~99	Mental and behavioural disorders
G00~99	Diseases of the nervous system
I00~99	Diseases of the circulatory system
J00~99	Diseases of the respiratory system
R00~99	Symptoms, signs and abnormal clinical and laboratory findings, not elsewhere classified

CAS results were used to estimate spatially distributed data on hourly air temperature T required as input in the Klima-Michel Model. This is, however, a complex algorithmic task, since the original design principle of CAS focused on structural rather than dynamical aspects of urban climate.

CAS considers two process regimes acting on different spatial scales, i.e. meso-scale and local-scale processes. The underlying assumption is that each place within a city with its specific urban characteristics shows cli-

matic modifications leading (besides others) to near-surface air temperatures that deviate more or less from a reference temperature of the city that is not (or only weakly) influenced by urban climate modifications. This means that the total air temperature deviation TD is the air temperature at a given place subtracted by a reference temperature. In CAS, TD is the sum of a meso-scale air temperature deviation MD and a local-scale air temperature deviation LD , assuming that the two process regimes are independent from each other, which may, in fact, not be perfectly the case.

It should be noted that MD , LD and TD are computed by the original CAS workflow as spatially varying nighttime variables to indicate heat-stress hazards rather than being meteorological variables (Yi et al. 2012). Therefore, empirical statistical relations are required to include MD , LD and TD in the analysis of hourly T fields for a specific day (here August 5, 2012).

The physically-based, non-hydrostatic numerical model MetPhoMod (Meteorology and Photochemistry Model, Perego 1999), implemented in CAS, was applied to compute MD as gridded values for both the SR and the DR. For this purpose, MetPhoMod simulations were performed for the three nested domains shown in Figure 1 using the one-way nesting option implemented in the model. Grid spacing was 2000 m in the MR, 500 m in the SR and 100 m in the DR. MetPhoMod does not allow for higher spatial resolutions than 100 m, and thus resolves only meso-scale processes leading to spatially varying air temperatures. The model set-up is shown in Table 2. The MR simulation only serves to define physically consistent lateral atmospheric boundary conditions for the MetPhoMod simulations for the SR and DR.

Air temperature values as obtained from the MetPhoMod simulations for the SR and DR were averaged between 20:00 and 06:00 KST to obtain nocturnal mean values for each grid point. The spatial average of the nocturnal mean air temperature in the SR served as reference temperature, i.e. was subtracted from the nocturnal mean value at each grid point to provide spatially distributed values for MD .

We used a GIS-based, spatially distributed, empirical-statistical model for computing LD . The GIS-based model conceptualises three different local-scale processes controlling LD : release of heat from the surface to the atmosphere (and vice versa) by sensible heat flux, dispersion of heat by turbulent mixing, and cooling of air due to cold-air production.

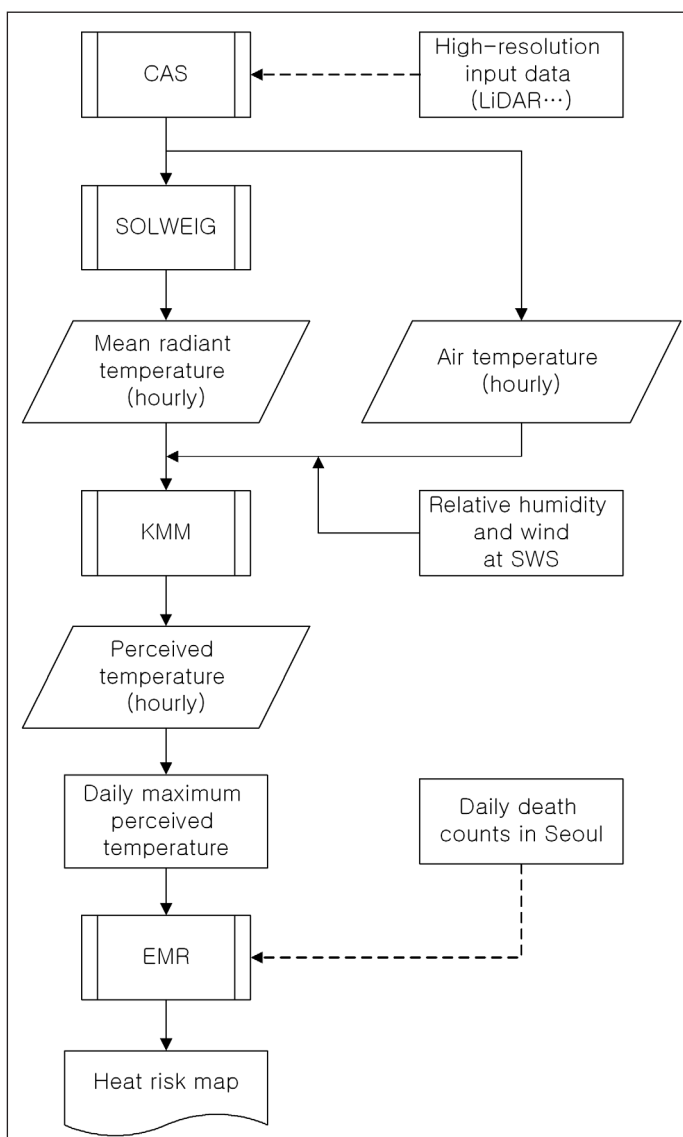


Fig. 4 Flowchart of the Biometeorological Climate impact Assessment System (BioCAS) comprising data and model results from its components CAS (Climate Analysis Seoul), the SOLWEIG (Solar Long Wave Environmental Irradiance Geometry) model, the KMM (Klima-Michel Model), and the EMR (Excess Mortality Rate) model.

Tab. 2 Model configuration and physics used in the MetPhoMod simulations

Category	Value(s)
Model domain	MR: Cartesian grid of 100 x 100 grid points, 2000 m grid spacing SR: Cartesian grid of 100 x 80 grid points, 500 m grid spacing DR: Cartesian grid of 80 x 60 grid points, 100 m grid spacing
Vertical layers	60 vertical layers between 10 and 6300 m a.s.l.
Surface properties	Surface height, albedo, emissivity, aerodynamic roughness length, volumetric heat capacity, thermal diffusivity, surface temperature and time-constant temperature at 1 m depth
Model physics	Air pressure non-hydrostatic, $k-\epsilon$ turbulence closure, full radiation and soil physics, wind advection, no clouds, no border dampening, no spatial filtering
Time period	Start: 21 June 06:00 KST, end: 22 June 18:00 KST; first 12 h discarded to remove spin-up effects
Time interval	Regular time steps of 10 s; adaptive time steps down to 1 s
Nesting	One way nesting MR -> SR -> DR; forcing data applied every 15 min
Initial conditions	No wind, i.e. $u = v = w = 0 \text{ ms}^{-1}$ Vertically constant virtual potential temperature = 20 °C Vertically constant mixing ratio = 0.4 g·kg ⁻¹ Surface temperature provided as spatially distributed values
Lateral boundary conditions (MR)	No wind, i.e. $u = v = w = 0 \text{ ms}^{-1}$ Virtual potential temperature of each vertical layer is set to layer mean value
Output variables	Data storage every 30 min: 3-dim: air pressure-, wind-, and air temperature fields 2-dim: wind-, and air temperature fields at 10 m above the momentum-absorbing surface 2-dim: full set of energy balance components (surface fluxes) and boundary layer variables

Following a study of *Christen and Vogt (2004)*, rural, suburban and urban sites show different mean values of the dimensionless ratio of sensible heat flux density and net radiation during nighttime depending on the complete surface aspect ratio f_{CSAR} , which is 1 for areas without buildings and larger than 1 for built-up areas, since their walls also contribute to the total surface. CAS estimates gridded f_{CSAR} values from data on fractional coverage of built-up surfaces f_{BS} and the mean height of buildings h_B by

$$f_{CSAR} = 1 + 4 \cdot \sqrt{f_{BS}} \cdot \frac{h_B}{ds} \quad (Eq. 1)$$

for an idealised building geometry with a single building per grid cell with four walls of equal size and a flat roof. Fractional coverage values f_{BS} and those for other land-cover types, as well as f_{CSAR} values were computed in CAS for grid cells of one hectare size centred on each grid point. Therefore, the grid cells have

an extent ds (100 m) that is much larger than the grid spacing (5 m) to consider local-scale effects stemming from land-cover variations in adjacent areas. Increasing f_{CSAR} values are assumed to lead to higher nocturnal sensible heat flux densities (*Christen and Vogt 2004*) and subsequent warming of high-density urban quarters, which is estimated by

$$dT_{SHF} = c_{SHF} \cdot (f_{CSAR} - 1) \quad (Eq. 2)$$

where dT_{SHF} is the local-scale increase in air temperature due to nocturnal sensible heat released by buildings into the atmosphere, and c_{SHF} is an empirical coefficient, which was set to a value of 2 K per unit increase in f_{CSAR} . Equation 2 ensures that air temperature in areas without buildings ($f_{CSAR} = 1$) remains unchanged. It should be noted that the choice of the value of c_{SHF} has to consider that warming of the air by nocturnal release of sensible

heat in built-up areas is partly already computed by the MetPhoMod simulations, thus dT_{SHF} only represents the unresolved local-scale contribution to nocturnal UHI formation.

Dispersion of heat in the nearby atmosphere by turbulent mixing smoothes the effect of sensible heat release such that the actual increase in air temperature dT'_{SHF} is smaller than dT_{SHF} for a point source, while adjacent areas will experience slightly increasing air temperatures. This effect is considered in CAS by convolving the gridded dT_{SHF} values with a Gaussian low pass kernel of 20x20 grid points, i.e. over an area of one hectare, to obtain gridded values for dT'_{SHF} .

The third effect considered in CAS for computing LD is local cooling due to cold-air production at rate Q_{ca} which is the volume of air that is cooled per unit area during one hour. CAS computes the decrease in air temperature by local cooling dT_{ca} by

$$dT_{ca} = c_{ca} \cdot Q_{ca} = c_{ca} \cdot (f_{TV} \cdot Q_{ca,TV} + f_{VS} \cdot Q_{ca,VS}) \quad (Eq. 3)$$

Here, only tall vegetation (TV) like forests or urban parks with trees and other vegetated surfaces (VS) are assumed to contribute to cold-air production by their fractional coverage values f_{TV} and f_{VS} , which were computed for one-hectare grid cells as for f_{BS} . $Q_{ca,TV}$ is the cold-air production rate for an area solely covered by TV, while $Q_{ca,VS}$ is the analogous value for VS. The values for $Q_{ca,TV}$ and $Q_{ca,VS}$ were estimated from literature references by $30 \text{ m}^3 \text{ m}^{-2} \text{ h}^{-1}$ and $15 \text{ m}^3 \text{ m}^{-2} \text{ h}^{-1}$, respectively (see e.g. Mosimann et al. 1999). The resulting Q_{ca} is multiplied by an empirical cooling factor, which was set to $-0.05 \text{ K m}^{-1} \text{ h}^{-1}$ in this study.

Finally, LD is computed as the sum of dT'_{SHF} and dT_{ca} . The term dT_{ca} illustrates that LD is mainly an indicator of local-scale nocturnal air temperature modifications since cold air production does not take place during daytime in summer.

Because MD , LD , and thus TD , are not meteorological variables but used as relative nocturnal heat-stress indicators, an additional empirical statistical procedure was developed to estimate the actual spatial distribution of T for summer days with calm winds and low cloud coverage on an hourly basis. We used hourly air temperature T_{SWS} observed at the SWS and spatially distributed differences between maximum air temperature T_{max} and the maximum air temperature $T_{max,SWS}$ at the SWS:

$$T = T_{SWS} + (T_{max} - T_{max,SWS}) + \varepsilon = T_{SWS} + dT_{max} + \varepsilon \quad (Eq. 4)$$

Differences in maximum air temperature dT_{max} are used in Equation 4 to minimise the residual term ε for times of hottest weather conditions. A stepwise regression was applied to estimate dT_{max} from a set of potential predictors, i.e. air temperature deviations MD , LD , TD , cold-air production rate Q_{ca} , fractional coverages f_{BS} , f_{TV} , f_{VS} , f_{US} , and f_{WS} , for the land cover classes including unvegetated surfaces (US) and water surfaces (WS), terrain elevation above sea level z , building height h_B , and the product of h_B and f_{BS} representing the building volume per unit area. The predictors are available as gridded data at a spatial resolution of 25 m for the SR and 5 m for the DR, respectively. The predictand values for dT_{max} were taken from the differences between maximum air temperatures observed at the 51 weather stations shown in Figure 3 and those at the SWS during the summer months (June, July and August) of the years between 2007 and 2011. Only those days during which the wind speed was in the lowest 25 % percentile, i.e. below 1.77 m/s, and cloud coverage in the lowest 30 % percentile were taken as input in the stepwise regression. In total, only eight days fulfilled the above-mentioned filter criteria. Predictor values were taken from the nearest grid points of the SR data.

The regression results, i.e. intercept and coefficients for those predictors finally considered in the regression model, were applied to all grid points in the DR to estimate dT_{max} , from which the hourly T distributions were finally estimated by applying Equation 4.

2.2.2 The Solar Long Wave Environmental Irradiance Geometry (SOLWEIG) model

The Solar Long Wave Environmental Irradiance Geometry model (SOLWEIG; Lindberg et al. 2008, Lindberg and Grimmond 2011) was used to simulate gridded hourly values for T_{mrt} in the DR based on a digital terrain model and digital surface models of buildings and vegetation at 5 m spatial resolution, along with hourly meteorological forcing data obtained from observations at the SWS on August 5, 2012 (Fig. 5). SOLWEIG is able to consider shadows due to buildings and vegetation. The 3D representation of vegetation in SOLWEIG includes a trunk zone. In this study, the trunk zone was assumed to be 25 % of the vegetation height. A transmissivity value of 0.02 for vegetation was chosen according to default values in SOLWEIG and the

results from *Konarska et al. (2013)*. Further, urban parameters were chosen according to the default values in SOLWEIG, i.e. albedo = 0.2, emissivity of walls = 0.9 and emissivity of ground = 0.95. SOLWEIG computed T_{mrt} for a standing man with short-wave absorption of 0.7 and long-wave absorption of 0.95.

2.2.3 The Klima-Michel Model (KMM)

The Klima-Michel Model (KMM) quantifies thermal conditions by computing PT , which is the temperature that a human would feel for a specific combination of ambient air temperature, relative humidity, solar radiation and wind speed. Therefore, it calculates the thermal balance between the human body and the surrounding environment, represented by T_{mrt} . Using PT as an indicator, human heat-stress levels can be standardised as a time fraction at extreme, strong and moderate thermal stress levels, which are >38, 32-38, 26-32 °C for PT , respectively (see e.g. *Staiger et al. 1997* and *2012* for further information on the KMM and on PT).

In this study, the gridded hourly T_{mrt} values simulated by the SOLWEIG model and the gridded hourly T val-

ues computed by *Equation 4* for the DR were used as input in the KMM along with hourly data on relative humidity and wind speed observed at the SWS. The KMM then provides gridded hourly PT values on output, from which PT_{max} is extracted at each grid point individually. The resulting PT_{max} values may thus be reached at different times during the day.

2.2.4 The Excess Mortality Rate (EMR) model

The impact of hot weather on human health was modeled as the estimated increase in mortality rates related to PT_{max} . Excess death rates r_{ED} for a given year y and day of year d were computed from total death rates r_{TD} of the same day using *Kysely's methods (2004)* to remove the trend of smaller death rates during weekends, as well as to remove intra- and inter-annual variations:

$$r_{ED}(y, d) = r_{TD}(y, d) - \overline{r_{TD}}(d) \cdot W(y, d) \cdot Y(y) \quad (Eq. 5)$$

Here, $r_{ED}(y, d)$ is computed on a daily basis as the difference between actual total death rate $r_{TD}(y, d)$ and ex-

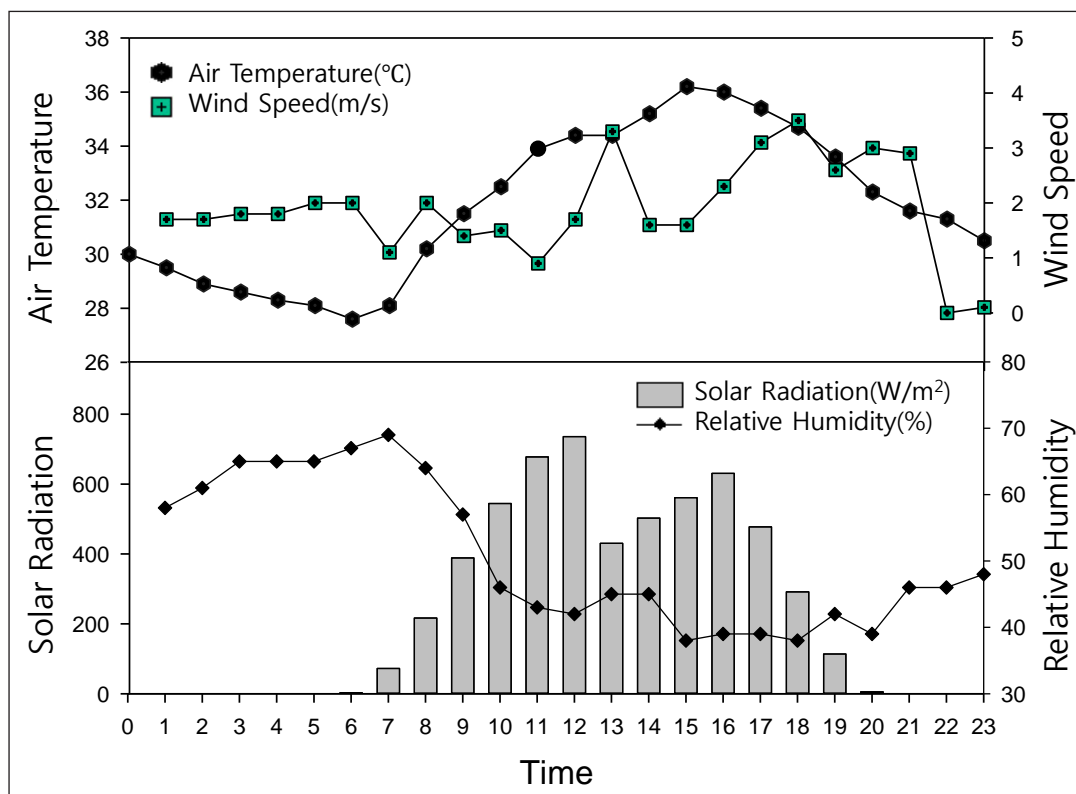


Fig. 5 Hourly weather conditions observed at the Seoul Weather Station (SWS) during the heat event on August 5, 2012

pected base death rate for the same day (the last term in Equation 5). The latter is defined as the product of mean daily total death rate $\bar{r}_{TD}(d)$, a correction factor $W(y,d)$ distinguishing between weekdays (1.005) and days during weekends (0.995), and a correction factor $Y(y)$ to consider inter-annual variations in death rates. $\bar{r}_{TD}(d)$ is the mean death rate for a given day of year d averaged over 21 years from 1991 to 2011, smoothed by a seven-day kernel centred on d . $Y(y)$ is computed as ratio of the mean death rate between June and September in a given year y and the mean death rate in the same period averaged for all years from 1991 to 2011. r_{EM} is then calculated from r_{ED} by

$$r_{EM}(y, d) = \frac{r_{ED}(y, d)}{\bar{r}_{TD}(d) \cdot W(y, d) \cdot Y(y)} \quad (\text{Eq. 6})$$

Expressing r_{EM} as increase in daily mortality rate relative to the expected base mortality rate of the same day yields two advantages. First, the ratio remains valid even in the case of underreporting of deaths or other errors in death counts, as long as there are no systematic differences in the errors for population groups showing different levels of vulnerability to heat stress. Second, r_{EM} does not depend on accurate data on population size, and is therefore also transferable to urban quarters of unknown number of residents. Absolute mortality rates for Seoul during June-September (mean value 1991-2011: $9.61 \cdot 10^{-6} \text{ d}^{-1}$) have been computed in this study by dividing the daily values of r_{ED} by the population of the same day, the latter being estimated from a second order curve of year-end resident numbers in Seoul (not shown).

3. Results and discussion

The results of this study are presented and discussed in the same sequence as in the previous chapter (methods) according to the workflow shown in Figure 4.

3.1 Climate Analysis Seoul (CAS)

Figure 5 presents the meteorological conditions observed at the SWS on August 5, 2012. On this day, air temperature did not fall below 27 °C and reached a maximum of 36 °C. Weak winds between 1 to 3 m/s and high values of solar radiation indicate the syn-

optic weather situation with low pressure gradients and low cloud coverage. Relative humidity was not exceptionally high, and its diurnal cycle was mainly controlled by air temperature.

The CAS models provided gridded data on MD , dT'_{SHF} and TD for both the SR (Fig. 6) and the DR Eunpyeong (Fig. 7). While the spatial distributions of MD are due to the combined effect of topography and land cover, the dT'_{SHF} patterns show the dominant control of land cover on nocturnal air temperature. As a consequence, TD combines the effects of altitude and land-cover variations. Figure 6 shows that the nocturnal UHI of Seoul is generally resolved by MetPhoMod and thus captured by MD . The nocturnal thermal pattern of Seoul shows strong spatial variability. The temperature range covered by TD is larger than 9 K. In some areas differences of more than 5 K are found in TD over short distances of a few hundred meters. Figure 7 reveals that both MetPhoMod (for MD) and the GIS-based models (for dT'_{SHF}) are able to resolve differences in the UHI intensity of the old, dense city quarters in the southern part of the DR (area A) and the less dense new town areas in the centre of the DR (area B). TD reveals that air temperature is about 1-2 K lower in the new town area than in the old town area.

The stepwise regression for estimating dT_{max} from gridded CAS data resulted in the optimal regression model formulated in Equation 7 (see below).

The intercept c_0 is 0.28 K, the values of the regression coefficients c_{MD} , c_{BS} , c_{TV} , c_{vol} and c_z are 1.18, 0.5 K, -0.8 K, -0.05 and -0.002 K/m, respectively. The explained variance r^2 is 0.42 ($N = 320$). The regression coefficients are significant at the $p = 0.20$ level.

The stepwise regression provides insight into some general processes controlling the thermal structure of Seoul during hot summer days. First, the intercept reveals that, on average, the SWS is about 0.3 K cooler than the other stations in Seoul during hot summer days, which shows that the cooling effect of large open spaces in cities is also weakly present during daytime, even when the fraction of TV is small.

Second, meso-scale thermal contrasts developing during nighttime as represented by MD are in parts

$$dT_{max} = c_0 + c_{MD} \cdot MD + c_{BS} \cdot f_{BS} + c_{TV} \cdot f_{TV} + c_{vol} \cdot h_B \cdot f_{BS} + c_z \cdot z + \varepsilon \quad (\text{Eq. 7})$$

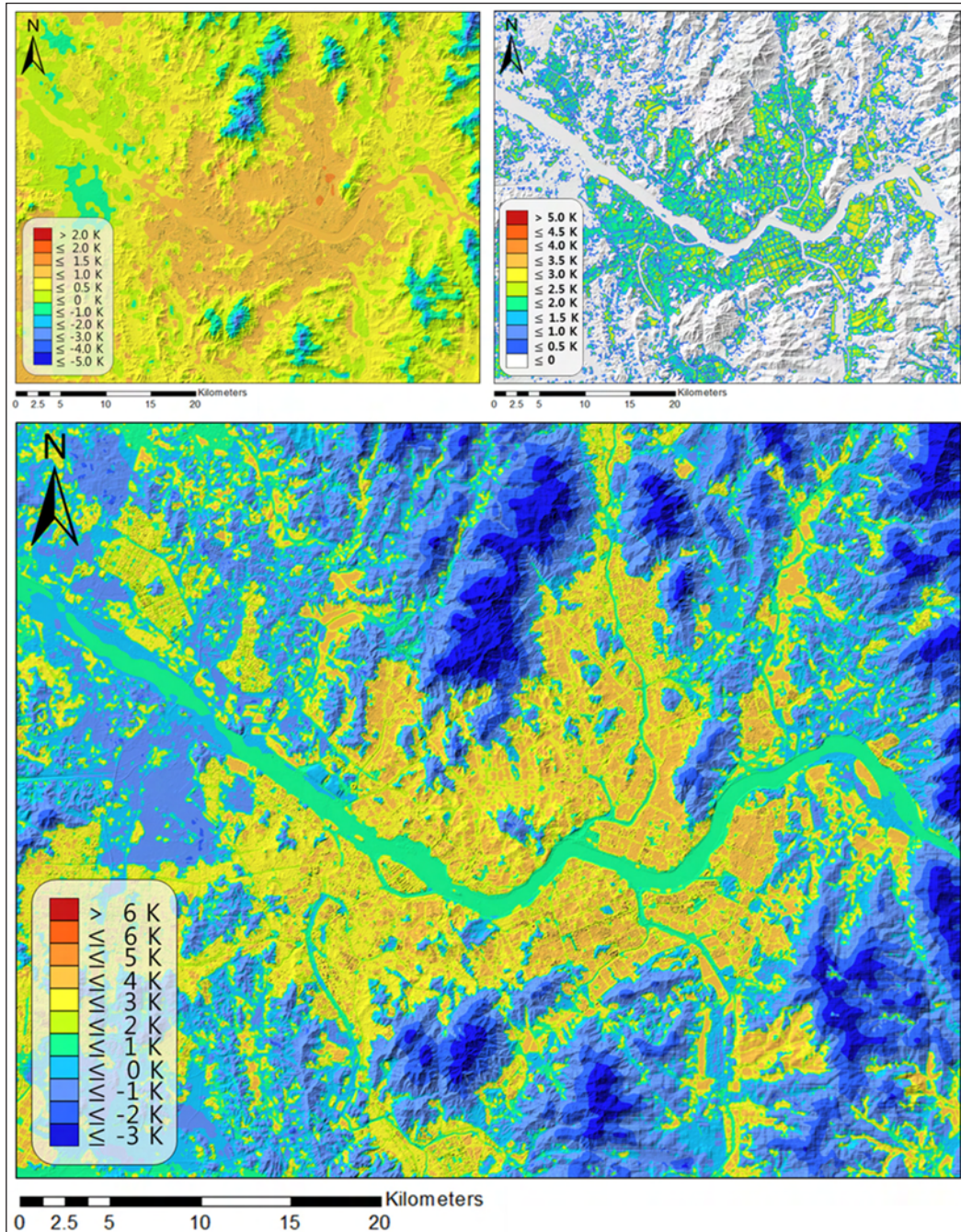


Fig. 6 Meso-scale air temperature deviation MD (upper left), local-scale increase in air temperature dT'_{SHF} due to nocturnal sensible heat released by buildings into the atmosphere considering dispersion by turbulent mixing (upper right) and total air temperature deviation TD (lower) in the Study Region (SR) calculated from the Climate Analysis Seoul (CAS). Hill shading indicates the mountainous topography.

also preserved during daytime, since MD was found to be a strong predictor for dT_{max} . This might not necessarily be solely the result of a memory effect, e.g. due to heat storage in buildings during daytime and subsequent heat release during nighttime, but could also be an indicator of similar climate controls during day and night (e.g. by topography). Our study is, however, not conclusive in this respect.

LD representing local-scale processes leading to nocturnal differences in air temperature in an aggregated manner was not included in the regression. Nevertheless, these processes are taken into account since separate predictors for the areal fractions of BS and TV, as well as for building volume per unit area ($h_B \cdot f_{BS}$) were considered by the stepwise regression. The regression coefficients

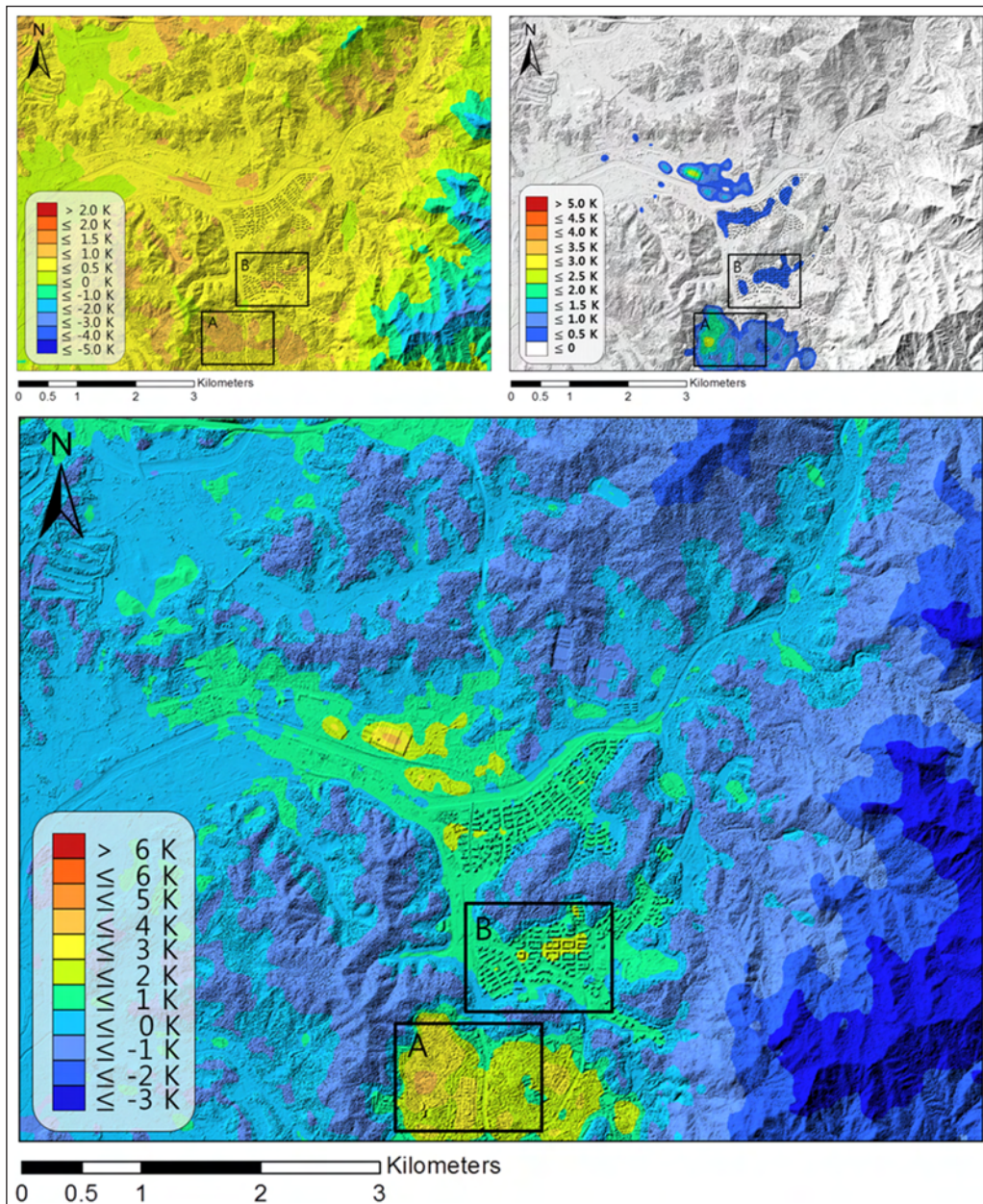


Fig. 7 Meso-scale air temperature deviation MD (upper left), local-scale increase in air temperature dT'_{SHF} due to nocturnal sensible heat released by buildings into the atmosphere considering dispersion by turbulent mixing (upper right) and total air temperature deviation TD (lower) in the Detail Region (DR) Eunpyeong calculated from the Climate Analysis Seoul (CAS). Hill shading indicates the mountainous topography. Tall apartment buildings in the center of the DR were constructed as part of a new town development.

for these predictors (i.e. c_{BS} , c_{TV} , c_{vol}) reveal that increasing building density leads to higher maximum air temperature, while tall vegetation leads to lower temperatures. Interestingly, higher building volumes per unit area also result in lower maximum air temperatures. The value of c_{vol} implies that an urban area with 50 % fractional coverage by 20 m tall buildings would experience maximum air temperatures that are 0.5 K lower due to this term in Equation 7. We assume that building shad-

ows are mainly responsible for this effect, but heat storage during daytime could also contribute to cooler air temperatures since it reduces the sensible heat flux into the atmosphere. For a given building density f_{BS} , building volume per unit area is directly proportional to building height h_B , thus shadow areas between buildings are larger when building volume is higher. Higher buildings would also increase f_{CSAR} and thus daytime storage heat flux into the buildings.

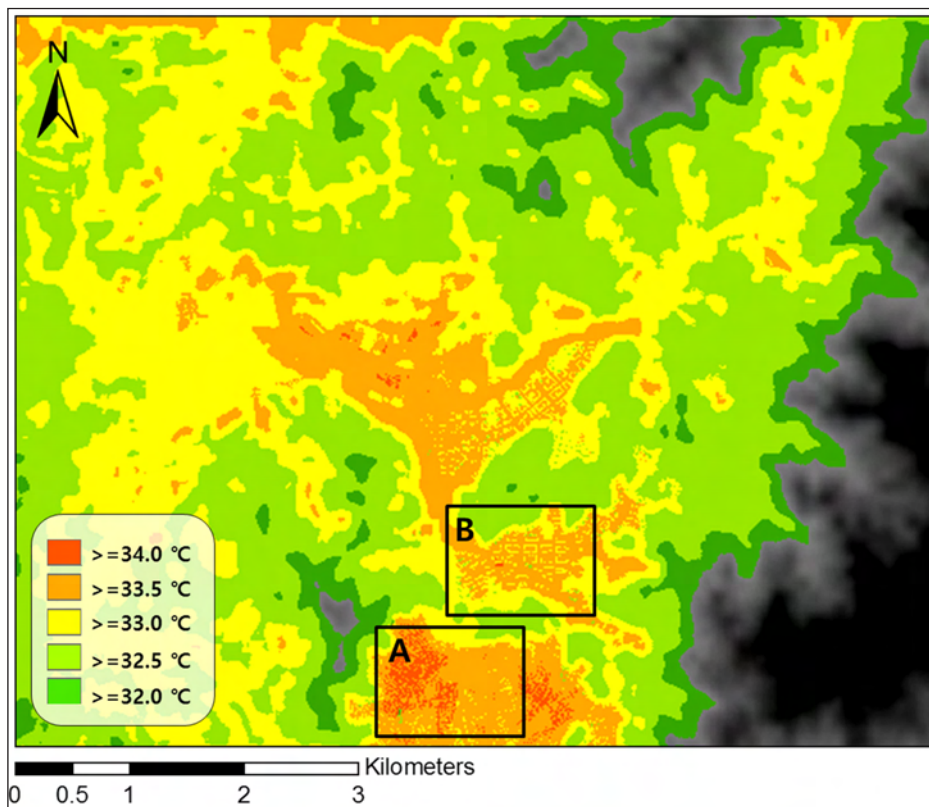


Fig. 8 Maximum air temperature in the Detail Region (DR) Eunpyeong, when a daily maximum temperature of 33°C would be recorded at the Seoul Weather Station (SWS) during a calm and sunny summer day. The A and B boxes represent old and new town areas in the DR.

Finally, the fact that altitude is also included in the stepwise regression indicates that MD possibly slightly underestimates lapse rates in Seoul (c_z is rather small). This is reasonable since the nocturnal residual layer is usually near-neutrally stratified while the lower part of the urban boundary layer is often characterised by unstable conditions during daytime. MD is, however, reflecting the nocturnal situation, and thus shows a less pronounced decrease of air temperature with altitude, which has to be compensated by the altitude-dependent term in Equation 7.

Figure 8 illustrates the application of the regression results for estimating the spatially distributed maximum air temperature in the DR by adding dT_{max} to a maximum air temperature of 33°C recorded at the SWS ($T_{max,SWS}$; see Eq. 4), which is used as threshold value for the heat wave advisory of the KMA. Both the old and new town areas showed higher maximum air temperatures than the SWS during calm and sunny summer days. Maximum air temperatures in the old town area are about 0.5 K higher than those in the new town area. This is mainly attributed to the higher building density of the old town area as compared to the new town area.

The results for dT_{max} were validated against observed temperature differences in the DR (NIMR 2012). In general, the spatial pattern of dT_{max} agrees well with observations, but the cooling effects by tall vegetation and building shadows are yet underestimated by dT_{max} . With respect to nighttime differences in air temperature as represented by TD , contrasts in maximum air temperature are much smaller. This has been shown by many urban climate studies (see e.g. Fenner et al. 2014).

3.2 The Solar Long Wave Environmental Irradiance Geometry (SOLWEIG) model

The results of the SOLWEIG model simulations are illustrated by the example shown in Figure 9, which displays the spatial pattern of T_{mrt} in the DR for 12:00 KST, the time when solar radiation is near to maximum values. Shadows provided either by buildings or trees strongly reduce T_{mrt} , while building roofs generally show highest values due to high sky view factors. This implies that shadows caused by buildings and trees not only slightly reduce air temperature but also strongly (and thus much more importantly) reduce T_{mrt} , which shows maximum differences of almost 30 K, partly over short distances.

3.3 The Klima-Michel Model (KMM)

The sequence of hourly patterns for air temperature and T_{mrt} was used as input in the KMM together with observed data on relative humidity and wind, resulting in hourly patterns of PT from which the spatial distribution of PT_{max} shown in Figure 10 was derived. Maximum differences in PT_{max} are about 20 K. The old and new town areas show strong differences in PT_{max} , with higher values in the old town areas, where only street canyons shadowed by buildings show intermediate values.

The large spatial contrast in PT_{max} and its spatial pattern reveal that spatial variations in T_{mrt} are the main driver in the KMM rather than air temperature variations (note that humidity and wind are not varying in space in this study). Thus, building-related controls on T_{mrt} also exert strongest influences on PT_{max} .

3.4 The Excess Mortality Rate (EMR) model

The statistical relation between PT_{max} and r_{EM} for hot days in Seoul (Fig. 11) was established by

$$r_{EM} = c_0 + c_1 \cdot PT_{max} + \varepsilon \quad (Eq. 8)$$

using data only for those days when PT_{max} exceeded the mean plus 2-sigma-value of the months June-September during the years 1983-2012 ($PT_{max} > 51.2^\circ\text{C}$). In total, 21 days fulfilled this criterion. The intercept c_0 is -9.07, the value of the regression coefficient c_1 is 0.178°C^{-1} . The explained variance r^2 is 0.565 ($N = 21$). The regression coefficient is significant at the $p = 0.05$ level.

The negative intercept is required to compensate the threshold value of 51.2°C for PT_{max} used in the regression. The regression coefficient c_1 shows that the population of Seoul responds very sensitive to

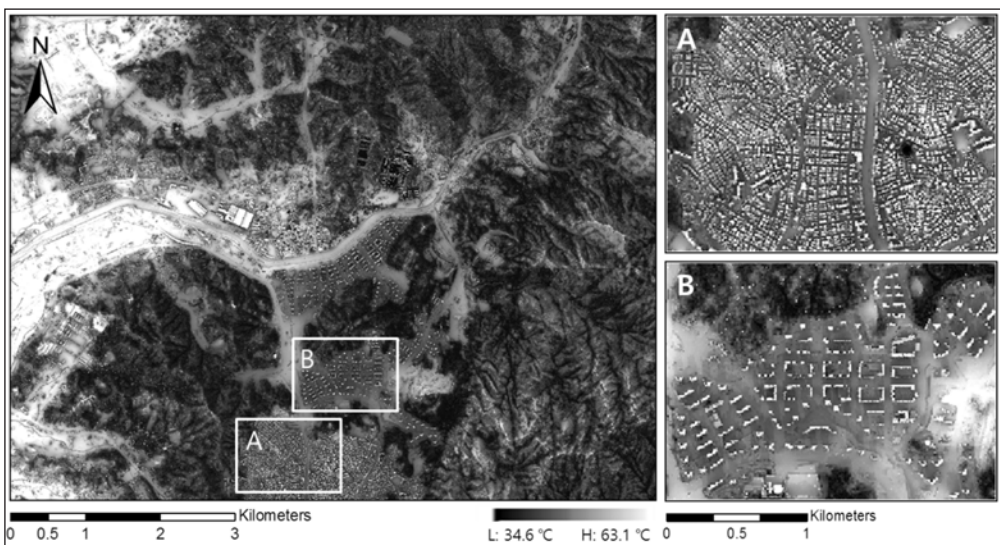


Fig. 9 Mean radiant temperature T_{mrt} in the Detail Region (DR) Eunpyeong during a heat wave event on August 5, 2012 12:00 KST. The A and B boxes represent old and new town areas.

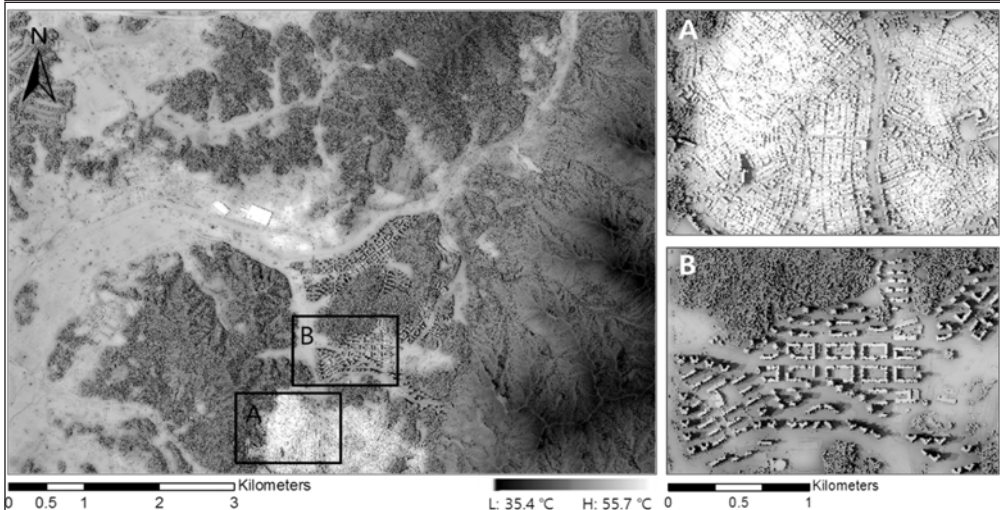


Fig. 10 Maximum perceived temperature PT_{max} in the Detail Region (DR) Eunpyeong during a heat wave event on August 5, 2012. The A and B boxes represent old and new town areas.

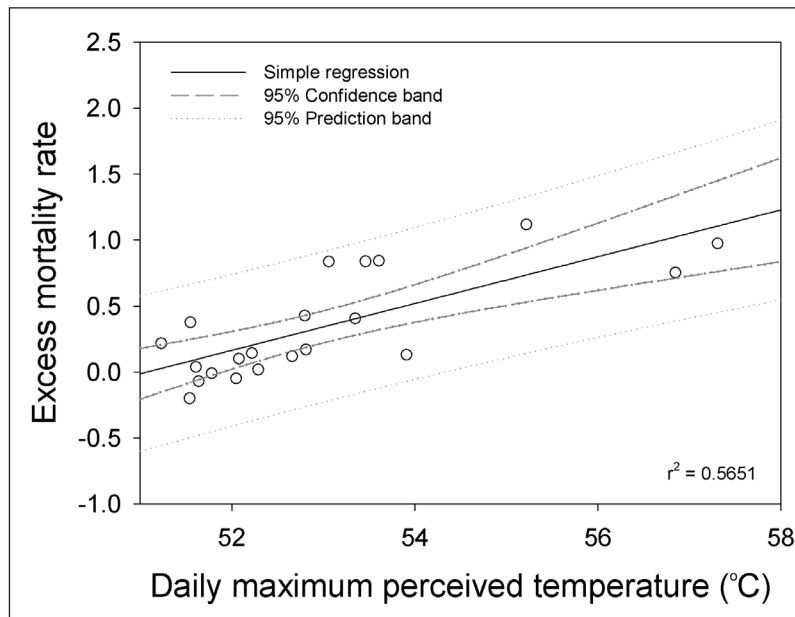


Fig. 11 Relationship between daily maximum perceived temperature PT_{max} and excess mortality rate r_{EM} , expressed as increase in daily mortality rate relative to the expected base mortality rate of the same day.

PT_{max} values exceeding the threshold: An increase in daily mortality of 10 % ($r_{EM} = 0.1$) is caused by only 0.57 K higher PT_{max} values.

The regression results were finally applied to compute spatially distributed values for r_{EM} for the DR Eunpyeong on August 5, 2012. Figure 12 displays the resulting r_{EM} patterns for the old (A) and new (B) town areas, while Table 3 summarises the statistical analyses for the same two areas. Both Figure 12 and Table 3 reveal that the old town area is much stronger affected by heat stress than the new town area. More than 14 % of the old town area is affected by excess mortality, while only about 0.1 % of the new town area is exposed to heat stress. The highest risk of heat-stress related mortality is located in the densely built-up quarters of the old town area.

Our major findings are in accordance to the results from other studies. For instance, Thorsson et al. (2004 and 2011) studied outdoor thermal conditions in an urban park and streets between buildings. They used predicted mean vote (PMV) and physiologically equivalent temperature (PET) in addition to T_{mrt} to assess human thermal comfort. Their studies showed the importance of urban geometry of buildings and parks with respect to heat stress in cities.

August 5, 2012 was one of the hottest days since 1991. The highest daily value of r_{EM} for entire Seoul

during the 21-year record was 1.12, observed on July 25, 1994. This day was part of a heat wave that started on July 16 and lasted until July 31. During all these days high excess mortality was observed. A mean r_{EM} value of 0.54 was recorded for the whole period. High PT_{max} values above the threshold of 51.2 °C were continuously observed at the SWS from July 22 to 29 causing an even higher mean excess mortality of 0.73. The maximum value of PT_{max} (57.3 °C) was recorded on July 24, while July 25 showed a lower value of 55.2 °C. This indicates that nocturnal thermal conditions during heat waves are also important. July 23 and 24 have been the only days in the whole 21-year record with daily means of PT exceeding 40 °C. Thus, there is a lagged response of r_{EM} not included in the EMR model. We argue that further improvements in the EMR model should consider a lagged response of r_{EM} on high PT values including nighttime conditions. This could be done e.g. by utilising the approach of analysing entire heat-wave events spanning over several days instead of individual hot days. This concept was introduced and successfully tested for Berlin by Scherer et al. (2013). One of the advantages of their analysis method would also be to remove the arbitrarily chosen percentile-based threshold for PT_{max} . In fact, there are numerous days in the 21-year period from 1991 to 2011 for which higher values of excess mortality are observed although PT_{max} stayed below 51.2 °C at the SWS.

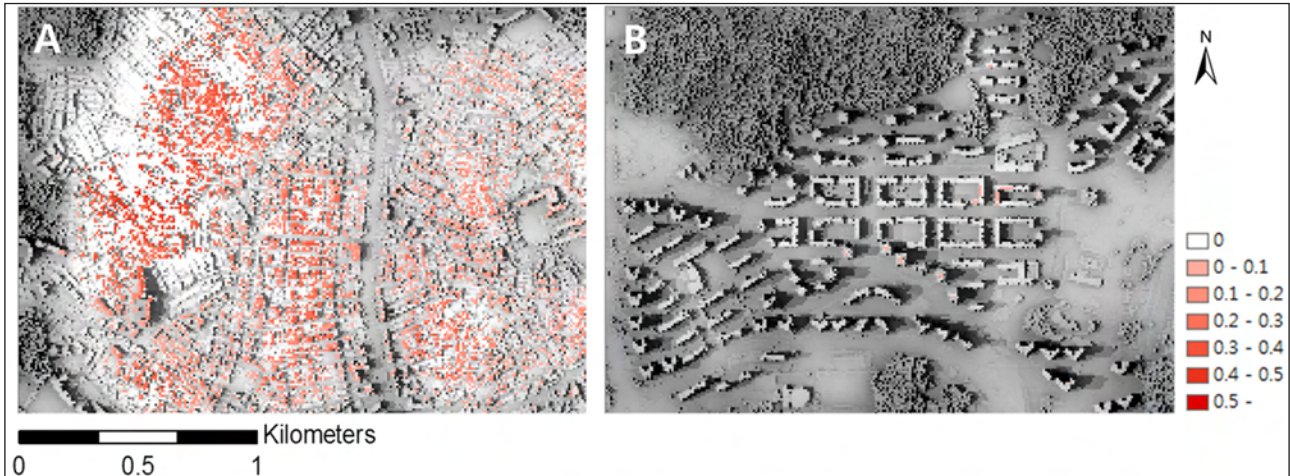


Fig. 12 Estimated excess mortality rate r_{EM} expressed as increase in daily mortality rate relative to the expected base mortality rate of the same day, during the heat event on August 5, 2012 for the old (A) and new (B) town areas in the Detail Region (DR) Eunpyeong.

4. Conclusions

We wanted to answer the question how the benefit of the urban design and development with respect to reducing heat-stress related mortality could be quantified. This is a long-lasting question in urban planning and (re-)development. Air temperature, wind flow and biometeorological models from conventional climate analyses can answer these questions, in part. The integration of biometeorological models in climate analyses provides further answers to this question with measurable and assessable figures.

The study illustrates that BioCAS can generally be applied for the quantification of the impacts of severe hot weather conditions on human health for different urban development scenarios with variable building morphologies and vegetation. We could reveal that urban re-development in an urban quarter of Seoul accomplished a reduction of heat-stress related mortality by about a half. BioCAS provides a basic framework for quantitative analysis of the urban climate and its consequences during urban design and planning to yield tangible figures of potential costs and benefits.

Nevertheless, further improvements of BioCAS are required in the future. In addition to the respective sug-

gestions already discussed in the previous chapter, it would be desirable to consider also indoor climate conditions evolving during heat waves causing heat stress. Therefore, high-resolution data would be necessary to assess the thermal response of buildings on ambient outdoor weather conditions to better characterise and quantify heat-stress hazards. In addition, spatially distributed data on socioeconomic status and population structure of local residents would lead to a better risk assessment, since then, differences in vulnerability to heat stress could also be considered. In Seoul, residents in old towns often show lower socioeconomic status and older age than people living in new towns. Therefore, excess mortality risks may be even higher than the BioCAS assessment reveals. Additional micro-scale measures like planting more tall roadside trees or installing screens over smaller streets without obstructing air ventilation in the street canyons could probably help to improve living conditions in these areas.

Acknowledgements

This research was supported by the “Advanced research on applied meteorology” and “Integrated weather services for urban and rural area” of the National Institute of Meteor-

Tab. 3 Minimum, maximum, mean and standard deviation (std. dev.) of excess mortality rates r_{EM} and areas affected by excess mortality in the old (A) and new (B) town areas in the Detail Region (DR) Eunpyeong

Area	Minimum	Maximum	Mean	Std. dev.	Area: $r_{EM} > 0$
Old town (A)	0	0.507	0.023	0.069	14.3 %
New town (B)	0	0.086	~ 0	0.001	0.1 %

logical Research (NIMR) / Korea Meteorological Administration (KMA). The study also contributes to the Research Unit 1736 "Urban Climate and Heat Stress in mid-latitude cities in view of climate change (UCaHS)" (www.UCaHS.org) funded by the Deutsche Forschungsgemeinschaft (DFG) under the codes SCHE 750/8-1 and SCHE 750/9-1. The authors would like to thank the editor and anonymous reviewers for their valuable comments that helped to substantially improve the manuscript.

References

- Akbari, H., S. Davis, S. Dorsano, J. Huang and S. Winnett (eds.) 1992: Cooling our communities. A guidebook on tree planting and light-colored surfacing. – U.S. EPA. – Washington
- Christen, A. and R. Vogt 2004: Energy and radiation balance of a central European city. – *International Journal of Climatology* **24** (11): 1395-1421
- Ebi, K.L., T.J. Teisberg, L.S. Kalkstein, L. Robinson and R.F. Weiher 2004: Heat watch/warning systems save lives: Estimated costs and benefits for Philadelphia 1995-98. – *Bulletin of the American Meteorological Society* **85** (8): 1067-1073
- Fenner, D., F. Meier, D. Scherer and A. Polze 2014: Spatial and temporal air temperature variability in Berlin, Germany, during the years 2001-2010. – *Urban Climate* (in press). – Online available at: <http://dx.doi.org/10.1016/j.uclim.2014.02.004>, 07/07/2014
- Gray, K.A. and M.E. Finster 2000: The urban heat island, photochemical smog, and Chicago: local features of the problem and solution. – U.S. EPA. – Washington. – Online available at: http://epa.gov/hiri/resources/pdf/the_urban_heat_island.pdf, 07/07/2014
- Harlan, S.L., A.J. Brazel, L. Prasad, W.L. Stefanov and L. Larson 2006: Neighborhood microclimates and vulnerability to heat stress. – *Social Science and Medicine* **63** (11): 2847-63
- Kalkstein, L.S. and J.S. Greene 1997: An evaluation of climate/mortality relationships in large U.S. cities and the possible impacts of a climate change. – *Environmental Health Perspectives* **105** (1): 84-93
- Kim, H., J.-S. Ha and J. Park 2006: High temperature, heat index, and mortality in 6 major cities in South Korea. – *Archives of Environmental and Occupational Health* **61** (6): 265-270
- Kim, J., K.R. Kim, B.-C. Choi, D.-G. Lee and J.-S. Kim 2009a: Regional distribution of perceived temperatures estimated by the human heat budget model (the Klima-Michel model) in South Korea. – *Advances in Atmospheric Sciences* **26** (2): 275-282
- Kim, J., D.-G. Lee and J. Kysely 2009b: Characteristics of heat acclimatization for major Korean cities. – *Atmosphere* **19** (4): 309-318 (in Korean with English abstract)
- Kim, K.R., L.S. Kalkstein, S.C. Sheridan, D.-G. Lee and Y.-J. Choi 2011a: The development of heat-health warning systems for Seoul: Is it feasible to divide the city into partitions? – *Proceedings of the 19th International Congress of Biometeorology*. – Auckland: 66-67
- Kim, Y.-M., S. Kim, H.-K. Cheong and E.-H. Kim 2011b: Comparison of temperature indexes for the impact assessment of heat stress on heat-related mortality. – *Environmental Health and Toxicology* **26**: e2011009
- Konarska, J., F. Lindberg, A. Larsson, S. Thorsson and B. Holmer 2013: Transmissivity of solar radiation through crowns of single urban trees – application for outdoor thermal comfort modelling. – *Theoretical and Applied Climatology*: Online first, DOI 10.1007/s00704-013-1000-3
- Kysely, J. 2004: Mortality and displaced mortality during heat waves in the Czech Republic. – *International Journal of Biometeorology* **49** (2): 91-97
- Kysely, J. and J. Kim 2009: Mortality during heat waves in South Korea, 1991 to 2005: How exceptional was the 1994 heat wave? – *Climate Research* **38** (2): 105-116
- Lee, D.-G., Y.-J. Choi, K.R. Kim, J.-Y. Byon, L.S. Kalkstein and S.C. Sheridan 2010: Development of heat-health warning system based on regional properties between climate and human health. – *Climate Change Research* **1**: 109-120 (in Korean with English abstract)
- Lindberg, F., B. Holmer and S. Thorsson 2008: SOLWEIG 1.0 – Modelling spatial variations of 3D radiant fluxes and mean radiant temperature in complex urban settings. – *International Journal of Biometeorology* **52** (7): 697-713
- Lindberg, F. and C.S.B. Grimmond 2011: The influence of vegetation and building morphology on shadow patterns and mean radiant temperatures in urban areas: model development and evaluation. – *Theoretical and Applied Climatology* **105** (3-4): 311-323
- Mosimann, T., T. Frey, and P. Trute 1999: Schutzgut Klima/Luft in der Landschaftsplanung. – *Informationsdienst Naturschutz Niedersachsen* **19** (4): 201-276
- Narumi, D., A. Kondo and Y. Shimoda 2009: Effects of anthropogenic heat release upon the urban climate in a Japanese megacity. – *Environmental Research* **109** (4): 421-431
- NIMR 2009: Understanding Climate Change (III). – National Institute of Meteorological Research. – Seoul (in Korean with English abstract)
- NIMR 2012: Annual Report of Advanced Research on Bio- and Industrial Meteorology. – National Institute of Meteorological Research. – Seoul (in Korean with English abstract)
- Oke, T.R. 1973: City size and the urban heat island. – *Atmospheric Environment* **7** (8): 769-779
- Perego, S. 1999: Metphomod – a numerical mesoscale model for simulation of regional photosmog in complex terrain: model description and application during Pollumet 1993

- (Switzerland). – *Meteorology and Atmospheric Physics* **70** (1-2): 43-69
- Scherber, K., M. Langner and W. Endlicher 2013: Spatial analysis of hospital admissions for respiratory diseases during summer months in Berlin taking bioclimatic and socio-economic aspects into account. – *DIE ERDE* **144** (3-4): 217-237
- Scherer, D. and W. Endlicher 2013: Editorial: Urban climate and heat stress – Part 1. – *DIE ERDE* **144** (3-4): 175-180
- Scherer, D., U. Fehrenbach, T. Lakes, S. Lauf, F. Meier and C. Schuster 2013: Quantification of heat-stress related mortality hazard, vulnerability and risk in Berlin, Germany. – *DIE ERDE* **144** (3-4): 238-259
- Shahmohamadi, P., A.I. Che-Ani, I. Etessam, K.N.A. Maulud and N.M. Tawil 2011: Healthy environment: the need to mitigate urban heat island effects on human health. – *Procedia Engineering* **20**: 61-70
- SMG 2009: Seoul Metropolitan Government Ordinance No. 4883 on Environmental Impact Assessment. – Online available at: <http://legal.seoul.go.kr/legal/english/front/page/law.html?pAct=lawView&pPromNo=406,07/07/2014>
- Staiger H., K. Bucher und G. Jendritzky 1997: Gefühlte Temperatur: Die physiologisch gerechte Bewertung von Wärmebelastung und Kältestress beim Aufenthalt im Freien mit der Maßzahl Grad Celsius. – *Annalen der Meteorologie* **33**: 100-107 (in German)
- Staiger H., G. Laschewski and A. Grätz 2012: The perceived temperature – a versatile index for the assessment of the human thermal environment. Part A: scientific basics. – *International Journal of Biometeorology* **56** (1): 165-176
- Thorsson, S., F. Lindberg, J. Björklund, B. Holmer and D. Rayner 2011: Potential changes in outdoor thermal comfort conditions in Gothenburg, Sweden due to climate change: the influence of urban geometry. – *International Journal of Climatology* **31** (2): 324-335
- Thorsson, S., M. Lindqvist and S. Lindqvist 2004: Thermal bioclimatic conditions and patterns of behaviour in an urban park in Göteborg, Sweden. – *International Journal of Biometeorology* **48** (3):149-156
- Tran, H., D. Uchihama, S. Ochi and Y. Yasuoka 2006: Assessment with satellite data of the urban heat island effects in Asian mega cities. – *International Journal of Applied Earth Observation and Geoinformation* **8** (1): 34-48
- U.S. EPA 2006: Excessive heat events guidebook. – U.S. EPA.– Washington. – Online available at: http://www.epa.gov/heatisland/about/pdf/EHEguide_final.pdf,07/07/2014
- Yi, C., J.-H. Eum, Y.-J. Choi, K.R. Kim, D. Scherer, U. Fehrenbach and G.-H. Kim 2011: Development of climate analysis Seoul (CAS) maps based on landuse and meteorological model. – *Journal of the Korean Association of Geographic Information Studies* **14**: 12-25 (in Korean with English abstract)
- Yi, C., S.-M. An, K.R. Kim, Y.-J. Choi and D. Scherer 2012: Improvement of air temperature analysis by precise spatial data on a local-scale – a case study of Eunpyeong New town in Seoul. – *Journal of the Korean Association of Geographic Information Studies* **15**: 144-158 (in Korean with English abstract)